

Framework-Substituted Lanthanide MCM-22 Zeolite: Synthesis and Characterization

Yajing Wu,^{†,§} Jun Wang,^{*,†,‡} Ping Liu,^{†,‡} Wei Zhang,^{†,‡} Jing Gu,^{†,‡} and Xiaojun Wang^{†,||}

State Key Laboratory of Materials-Oriented Chemical Engineering, College of Chemistry and Chemical Engineering, College of Sciences, and College of Materials Science and Engineering, Nanjing University of Technology, Nanjing 210009, China

Received August 24, 2010; E-mail: junwang@njut.edu.cn

Abstract: Incorporation of Ce and La into the framework of MCM-22 zeolite has been achieved by cohydrolysis and condensation of tetraethylorthosilicate and lanthanide salts in moderate/weak acidic media followed by a switch of synthesis gels to basic conditions for hydrothermal crystallization. The promotion effect of the framework Ce (La) when Ce(La)-MCM-22 serves as the catalyst support for hydroisomerization of *n*-heptane is demonstrated. Framework substitutions of lanthanides are evidenced by a set of mutually complementary characterizations, catalytic tests, and item-by-item comparisons with the impregnated and ion-exchanged counterparts. The novel synthesis strategy may give further outlines for the production of other types of heteroatomic zeolites.

As a class of crystalline aluminosilicates, zeolites have been widely applied as catalysts in the refining, petrochemical, and fine-chemical industries.¹ Incorporation of transition metals into zeolite frameworks results in heteroatomic zeolites that access new catalytic applications.² Although lanthanides are well-known catalyst additives,³ synthesis of framework-substituted lanthanide zeolites still remains as a huge challenge because of their much larger ionic radii in comparison with Si⁴⁺.

For the synthesis of heteroatomic zeolites, conventional hydrothermal crystallization,⁴ the dry-gel route,⁵ fluoride modification,⁶ and microwave-assisted procedures⁷ have been employed. Silica sources, solvents, templates, promoters (inhibitors), temperature, time, pH, etc., influence the synthesis significantly.⁸ In previous efforts, hydrolysis of silica and metal sources for preparing synthesis gels and the succeeding hydrothermal crystallization have always been conducted in strongly basic media,¹ where metal ions tend to be converted into highly condensed species and have fewer chances to link with silanol groups to produce isolated tetracoordinated blocks, the primary zeolite-forming units. Thus, the existing approaches are experiential and short of prediction.

It is known that silica sources such as tetraethylorthosilicate (TEOS) can be hydrolyzed in both basic and acidic media.⁹ Actually, mesoporous molecular sieves can be synthesized in acidic media;¹⁰ however, it is difficult to insert metal (M) ions into silicious pore walls because of the facile dissociation of M–O–Si bonds due to the employed strong acidity.¹¹ In contrast, the synthesis of zeolites involving the hydrolysis of silica sources in acidic media has been largely overlooked.¹²

Herein, we propose the following strategy to incorporate lanthanide into zeolite frameworks. TEOS and lanthanide are first

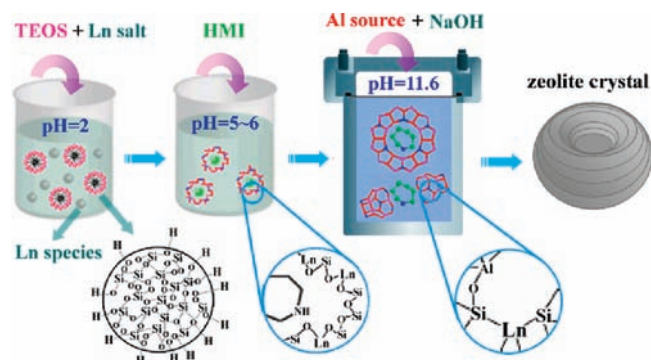


Figure 1. Schematic diagram of the synthesis procedure for framework-substituted lanthanide MCM-22 zeolite.

cohydrolyzed under moderately acidic conditions (pH ~2) to facilitate the isolation and dispersion of metal ions. Next, the conditions are adjusted to weakly acidic (pH 5–6) by adding a basic template. Finally, the resulting gel is switched to the conventional basic conditions for hydrothermal crystallization. The key of this “acidic cohydrolysis route” is to hydrolyze and condense TEOS and lanthanide under moderately/weakly acidic conditions, aiming to create the Si–O–M–O–Si linkage around the templates, which is the precondition for generating the primary tetracoordinated structural blocks for a zeolite.

Accordingly, we report the synthesis of framework-substituted lanthanide MCM-22 zeolites, denoted as Ln-MCM-22(*n*) (Ln = La or Ce; *n* = Si/Ln molar ratio in the synthesis), using the procedure sketched in Figure 1. Impregnated and ion-exchanged Ln-containing MCM-22 samples, respectively designated as Ln-Im-M22(*n*) (*n* defined as above) and Ln-Ex-M22, were also prepared for comparison. They were characterized by X-ray diffraction (XRD), scanning electron microscopy (SEM), FT-IR and UV–vis spectroscopy, thermogravimetric analysis (TGA), ²⁹Si magic-angle-spinning (MAS) NMR spectroscopy, inductively coupled plasma–atomic emission spectroscopy (ICP–AES), and Brunauer–Emmett–Teller (BET) surface area analysis. The catalytic performance was tested using the hydroisomerization of *n*-heptane.

The XRD patterns for as-calcined Ln-MCM-22 [Figure 2A,B; also see Figure S1 in the Supporting Information (SI) for as-synthesized samples] displayed featured peaks assigned to the MWW structure,¹³ and they all showed BET surface areas of ~500 m² g⁻¹ (Table S1 in the SI), demonstrating the production of good a MCM-22 phase. Moreover, the unit-cell volume for the as-calcined Ce(La)-MCM-22 in Table S1 increased monotonically with Ce and La loadings. This is indicative of the insertion of Ln ions into TO₄ (T = tetrahedrally bonded cation) sites,⁴ consistent with the much larger radii of Ce (0.1034 nm) and La (0.1061 nm) ions in comparison with Si⁴⁺ (0.040 nm). In contrast, no increment of

[†] State Key Laboratory of Materials-Oriented Chemical Engineering.

[‡] College of Chemistry and Chemical Engineering.

[§] College of Sciences.

^{||} College of Materials Science and Engineering.

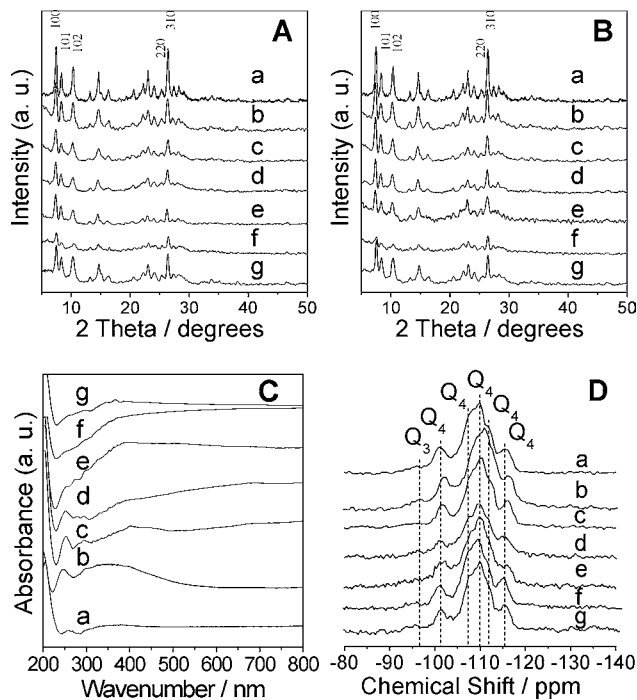


Figure 2. (A, B) XRD patterns for as-calcined (A) Ce-MCM-22 and (B) La-MCM-22: (a) MCM-22, (b) Ln-MCM-22(400), (c) Ln-MCM-22(100), (d) Ln-MCM-22(50), (e) Ln-MCM-22(30), (f) Ln-Im-M22(100), (g) Ln-Ex-M22. (C) UV-vis spectra for as-calcined samples: (a) MCM-22, (b) La-MCM-22(400), (c) La-MCM-22(100), (d) La-MCM-22(50), (e) La-MCM-22(30), (f) La-Im-M22(100), (g) La-Ex-M22. (D) ²⁹Si MAS NMR spectra of as-calcined samples: (a) MCM-22, (b) Ce-MCM-22(30), (c) La-MCM-22(30), (d) Ce-Im-M22(100), (e) Ce-Ex-M22, (f) La-Im-M22(100), (g) La-Ex-M22.

the unit cell volume was detected for Ce(La)-Im-M22 and Ce(La)-Ex-M22. SEM images (Figures S2 and S3) illustrate very similar morphologies but larger crystals of Ln-MCM-22 in comparison with neat MCM-22.^{12,14}

In the TGA of Ln-MCM-22 (Figure S4), the initial weight loss up to 180 °C was due to desorption of physically adsorbed water, while the decomposition of hexamethyleneimine (HMI, the template in the synthesis) took place at 227–650 °C.¹⁵ The total weight loss for HMI increased with the Ce and La loadings (Table S1), implying that a fraction of the HMI species are in protonated form to neutralize the excessive negative charges due to the presence of the framework trivalent Ln ions.¹⁶

The FT-IR spectra of the as-synthesized samples (Figure S5A) indicated that the band at 1086 cm⁻¹ for ν_{as}(Si–O–Si) of pure MCM-22¹⁷ moved to 1081 cm⁻¹ for Ce-MCM-22(50) and 1082 cm⁻¹ for La-MCM-22(50), respectively, strongly suggesting the incorporation of Ce and La into the framework.¹⁸ Moreover, the FT-IR spectra of the as-calcined samples told the same story; nevertheless, for impregnated and ion-exchanged samples, the bands for ν_{as}(Si–O–Si) reversely shifted to higher wavenumbers (Figure S5B).

In the UV-vis spectra in Figure 2C, La-MCM-22 gave a main band at ~255 nm due to the tetrahedral La(III) ions and a less intense shoulder at ~400 nm arising from the coexistence of extraframework La₂O₃ nanocrystallites.¹⁹ However, no peak assigned to tetrahedral framework La(III) sites was detectable for La-Im-M22 and La-Ex-M22. On the other hand, Ce-MCM-22 (Figure S6) showed a broad absorption band at ~300 nm due to the presence of the well-dispersed tetracoordinated Ce(IV) centers and a weak shoulder at ~250 nm assignable to tetrahedral Ce(III) sites.¹⁸

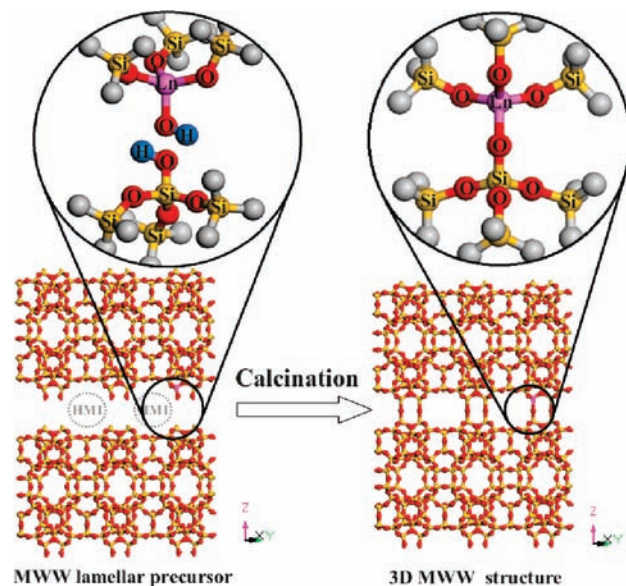


Figure 3. Structural change in the calcination of as-synthesized Ln-MCM-22 and proposal for the possible position of framework Ln ions.

The ²⁹Si MAS NMR spectra in Figure 2D displayed five peaks between –101 and –116 ppm attributable to Q⁴ [(Si(0 M)] sites and one peak at –96 ppm due to Q³ [Si(1 Me)] sites.²⁰ Both the chemical shifts and curved shapes of the impregnated and ion-exchanged samples were almost identical to those of neat MCM-22, while those of Ce(La)-MCM-22 changed clearly. The peaks for Ce(La)-MCM-22 were shifted upfield relative to those of their Al analogue, suggesting the incorporation of Ln ions into the MCM-22 framework.²¹ In addition, the apparent overlap of the bands in the Q⁴ range for Ce-MCM-22 is mostly due to the paramagnetic effect of framework Ce(III) ions evidenced by the TGA and UV-vis results.

Because of the much longer bond length of Ce–O (0.243 nm) and La–O (0.254 nm) in comparison with Si–O (0.161 nm), the incorporation of Ce and La into TO₄ sites should be extremely difficult. Despite this consideration, all of the above mutually complementary characteristics, together with item-by-item comparisons with the impregnated and ion-exchanged counterparts, demonstrate the incorporation of Ce and La into the framework of MCM-22 via the “acidic cohydrolysis route” developed in this study.

Figure 3 depicts the structural change in the calcination of 2D MWW lamellar precursors, where the position of Ln ions in framework sites is proposed. For neat MCM-22, the as-synthesized lamellar precursor consists of silicate layers linked together by the HMI template along the *c* axis.¹⁵ A hexagonal array of pockets with 12-membered-ring openings is exposed on the external surface of the layers. On both sides of the layer, these pockets have fully connected terminal TO₄ sites, with one of the four coordination positions being linked with hydroxyl. A subsequent calcination produces the final 3D MWW structure through simultaneous elimination of occluded HMI molecules and interlayer dehydroxylation.¹⁵ For as-synthesized Ln-MCM-22, Ln ions most possibly occupy terminal sites on the external surface of the 2D MWW layer, and in this case, the high tetrahedral tension in the LnO₄ units arising from the large radii of the Ln ions could be relaxed by the coordination with a hydroxyl group. Since the formation of Si–O–M bridges is energetically more favorable than that of Si–O–Si,²² it is reasonable to suppose that upon calcination, the hydroxyls linked with the terminal Ln ions are able to react with

Table 1. Catalytic Performance of Pt/Ln-MCM-22(*n*) and Control Catalysts for Hydroisomerization of *n*-Heptane^a

catalyst	conv. (%) ^b	product selectivity (%)			
		monoiso. ^c	multi-iso. ^d	cra. ^e	cyc. ^f
Pt/MCM-22	29.2	90.1	3.4	5.6	0.9
Pt/La-MCM-22(400)	41.2	91.2	2.5	5.2	1.1
Pt/La-MCM-22(100)	46.4	92.2	3.5	3.7	0.6
Pt/La-MCM-22(50)	29.8	83.1	6.7	9.3	0.9
Pt/La-Im-M22(400)	28.2	91.1	2.3	5.1	1.5
Pt/La-Im-M22(100)	31.6	88.5	6.0	5.0	0.5
Pt/La-Im-M22(50)	21.0	91.6	2.0	4.3	2.1
Pt/La-Ex-M22	25.8	87.0	6.2	6.0	0.8
Pt/Ce-MCM-22(400)	45.8	91.7	2.5	4.8	1.0
Pt/Ce-MCM-22(100)	56.4	92.0	3.4	4.1	0.5
Pt/Ce-MCM-22(50)	46.4	90.4	3.5	5.6	0.5
Pt/Ce-Im-M22(400)	29.9	91.6	2.2	4.8	1.4
Pt/Ce-Im-M22(100)	38.0	83.6	8.4	7.5	0.5
Pt/Ce-Im-M22(50)	23.2	90.9	2.2	5.0	1.9
Pt/Ce-Ex-M22	28.1	88.4	5.3	5.6	0.7

^a Reaction conditions: temperature, 200 °C; weight hourly space velocity, 2.1 h⁻¹; H₂/*n*-heptane molar ratio, 7.9; time on-stream, 2 h. ^b Conversion of *n*-heptane. ^c Selectivity for monobranched isoheptanes. ^d Selectivity for multibranched isoheptanes. ^e Selectivity for cracking products. ^f Selectivity for cyclization products.

the surface silanol groups from the nearby layer to create the Si–O–Ln linkages. Consequently, the 3D MWW structure containing the framework Ln ions is obtained. This proposal is in agreement with the gradual and substantial expansion of the unit cell volume observed in Table S1.

The synthesis of Sm-MCM-22(100) using the same acidic cohydrolysis route confirmed the above findings (Figure S7 and Table S2), though the broad UV–vis band beyond 400 nm showed coexistence of extraframework Sm oxides.²³

The numerous applications of existing heteroatomic zeolites encouraged us to evaluate the catalytic activity of Ln-MCM-22. Pt/Ln-MCM-22 (0.4 wt % Pt loading) were thus prepared as bifunctional catalysts for hydroisomerization of *n*-heptane [see Figure S8 for optimization of reaction conditions over Pt/Ln-MCM-22(100)], a reaction important for advanced liquid fuels.²⁴ Over all of the catalysts, isoheptanes were the dominant products, and the selectivity for monobranched isomers was always as high as ~90% (Table 1), which is consistent with the previous viewpoint that monobranched alkanes are capable of diffusing through the 10-membered-ring windows connecting the large cavities of MCM-22, whereas multibranched ones are not.²⁵ Comparison of conversions shows that the members of the Pt/Ln-MCM-22(*n*) series were much more active than their parent Pt/MCM-22. However, at a high La loading (*n* = 50), the conversion dropped, largely as a result of the very clear appearance of extraframework La₂O₃ shown in Figure 2C. Moreover, when the Ln loadings were the same (*n* = 400, 100, or 50), Pt/La(Ce)-MCM-22(*n*) were substantially more active than the impregnated counterparts Pt/La(Ce)-Im-M22(*n*). In addition, at very low Ln loadings, the ion-exchanged Pt/La(Ce)-Ex-M22 showed much lower conversions than Pt/La(Ce)-MCM-22(400). These reaction results indicate that the framework-substituted Ln ions in MCM-22 do act as catalytic promoters for this reaction, whereas extraframework ones such as those in the impregnated and ion-exchanged Ln oxides/ions do not.

Metals and acidic sites of zeolite-supported noble-metal bifunctional catalysts are known active centers for hydroisomerization of alkanes, but nevertheless, the zeolite pore structure also significantly influences the activity.²⁶ Framework substitution of Ln ions into MCM-22 expands the cell volume and thus facilitates the access

of reactants to the active centers in microchannels, including the acidic sites relative to TO₄ Ln ions. However, impregnated and ion-exchanged Ln oxides/ions inevitably narrow the micropores of MCM-22, which balances out the possible beneficial Ln modifications of the acidic sites, and therefore, no catalytic promotion effect was observed in the case of these extraframework Ln modifications.

In summary, framework-substituted lanthanide zeolites have been synthesized by the “acidic cohydrolysis route” developed in this study (i.e., cohydrolysis and condensation of TEOS and a lanthanide salt in moderately/weakly acidic media followed by switching the resulting synthesis gels to a conventional basic environment just before the onset of the succeeding hydrothermal crystallization). This strategy has been demonstrated by the synthesis of framework-substituted Ce(La)-MCM-22. The present results may give further outlines for the synthesis of other types of heteroatomic zeolites.

Acknowledgment. This work was supported by the National Natural Science Foundation of China (20776069, 20976084).

Supporting Information Available: Experimental details, Figures S1–S8, and Tables S1 and S2. This material is available free of charge via the Internet at <http://pubs.acs.org>.

References

- Cundy, C. S.; Cox, P. A. *Chem. Rev.* **2003**, *103*, 663–702.
- (a) Fricke, R.; Kosslick, H.; Lischke, G.; Richter, M. *Chem. Rev.* **2000**, *100*, 2303–2406. (b) Fan, W.; Snyder, M. A.; Kumar, S.; Lee, P.-S.; Yoo, W. C.; McCormick, A. V.; Penn, R. L.; Stein, A.; Tsapatsis, M. *Nat. Mater.* **2008**, *7*, 984–991. (c) Astala, R.; Auerbach, S. M. *J. Am. Chem. Soc.* **2004**, *126*, 1843–1848.
- (a) Marcilly, C. *J. Catal.* **2003**, *216*, 47–62. (b) Tagliaferri, S.; Köppel, R. A.; Baiker, A. *Ind. Eng. Chem. Res.* **1999**, *38*, 108–117.
- Fan, W.; Wu, P.; Namba, S.; Tatsumi, T. *Angew. Chem., Int. Ed.* **2004**, *43*, 236–240.
- Ke, X.; Xu, L.; Zeng, C.; Zhang, L.; Xu, N. *Microporous Mesoporous Mater.* **2007**, *106*, 68–75.
- Brigden, C. T.; Thompssett, D.; Williams, C. D. *Dalton Trans.* **2004**, 2829–2830.
- Hwang, Y. K.; Chang, J.-S.; Park, S.-E.; Kim, D. S.; Kwon, Y.-U.; Jung, S. H.; Hwang, J.-S.; Park, M. S. *Angew. Chem., Int. Ed.* **2005**, *44*, 556–560.
- Fan, W.; Duan, R.; Yokoi, T.; Wu, P.; Kubota, Y.; Tatsumi, T. *J. Am. Chem. Soc.* **2008**, *130*, 10150–10164.
- Baney, R. H.; Itoh, M.; Sakakibara, A.; Suzuki, T. *Chem. Rev.* **1995**, *95*, 1409–1430.
- Zhao, D.; Feng, J.; Huo, Q.; Melosh, N.; Fredrickson, G. H.; Chmelka, B. F.; Stucky, G. D. *Science* **1998**, *279*, 548–552.
- Wu, S.; Han, Y.; Zou, Y. C.; Song, J. W.; Zhao, L.; Di, Y.; Liu, S. Z.; Xiao, F. S. *Chem. Mater.* **2004**, *16*, 486–492.
- Wu, Y.; Ren, X.; Wang, J. *Mater. Chem. Phys.* **2008**, *113*, 773–779.
- Lenonwicz, M. E.; Lawton, J. A.; Lawton, S. L.; Rubin, M. K. *Science* **1994**, *264*, 1910–1913.
- Hu, G.; Ma, D.; Liu, L.; Cheng, M.; Bao, X. H. *Angew. Chem., Int. Ed.* **2004**, *43*, 3452–3456.
- Lawton, S. L.; Fung, A. S.; Kennedy, G. J.; Alemany, L. B.; Chang, C. D.; Hatzikos, G. H.; Lissy, D. N.; Rubin, M. K.; Timken, H.-K. C.; Steuernagel, S.; Woessner, D. E. *J. Phys. Chem.* **1996**, *100*, 3788–3798.
- Catherine, I. R.; Craig, D. W.; Catherine, V. A. D. *Chem. Commun.* **1997**, 1849–1850.
- Corma, A.; Corell, C.; Fornés, V.; Kolodziejski, W.; Pérez-Pariente, J. *Zeolites* **1995**, *15*, 576–582.
- Dai, Q.; Wang, X.; Chen, G.; Zheng, Y.; Lu, G. *J. Catal.* **2002**, *207*, 213–223.
- Zhan, W. C.; Guo, Y. L.; Wang, Y. Q.; Liu, X. H.; Guo, Y.; Wang, Y. S.; Zhang, Z. G.; Lu, G. Z. *J. Phys. Chem. B* **2007**, *111*, 12103–12110.
- Kennedy, G. J.; Lawton, S. L.; Rubin, M. K. *J. Am. Chem. Soc.* **1994**, *116*, 11000–11003.
- Kim, S. J.; Jung, K.-D.; Joo, O.-S. *J. Porous Mater.* **2004**, *11*, 211–218.
- Ermoshin, V. A.; Smirnov, K. S.; Bougeard, D. *THEOCHEM* **1997**, *393*, 171–176.
- Zhu, W.; Xu, L.; Ma, J.; Yang, R.; Chen, Y. *J. Colloid Interface Sci.* **2009**, *340*, 119–125.
- Liu, P.; Wang, J.; Zhang, X.; Wei, R.; Ren, X. *Chem. Eng. J.* **2009**, *148*, 184–190.
- Denayer, J. F. M.; Ocakoglu, R. A.; Thybaut, J.; Marin, G.; Jacobs, P.; Martens, J.; Baron, G. V. *J. Phys. Chem. B* **2006**, *110*, 8551–8558.
- Ravishanker, R.; Sivasanker, S. *Appl. Catal., A* **1996**, *142*, 47–59.

JA107633J